RESEARCH

Potential functions and mechanisms of lysine crotonylation modification (Kcr) in tumorigenesis and lymphatic metastasis of papillary thyroid cancer (PTC)

Zhaokun Li[1], Jingting Li[1], Fang Li[1], Liang Han[2], Chengqiu Sui[1], Le Zhou[1], Daqi Zhang[1], Yantao Fu[1], Rui Du[1], Jiedong Kou[1], Gianlorenzo Dionigi[3], Hui Sun[1]* and Nan Liang[1]*

Abstract

Objectives To examine the putative functions and mechanisms of lysine crotonylation (Kcr) during the development and progression of papillary thyroid cancer (PTC).

Methods Samples of thyroid cancer tissues were collected and subjected to liquid chromatography–tandem mass spectrometry. Crotonylated differentially expressed proteins (DEPs) and differentially expressed Kcr sites (DEKSs) were analyzed by Motif, dynamic expression model analysis (Mfuzz), subcellular localization, Kyoto Encyclopedia of Genes and Genomes (KEGG) pathway annotation, Go Ontology (GO) annotation, and protein–protein interaction analysis (PPI). Validation was performed by immunohistochemistry (IHC).

Results A total of 262 crotonylated DEPs and 702 DEKSs were quantitated. First, for the tumor/normal comparison, a dynamic expression model analysis (Mfuzz) of the DEKSs revealed that clusters 1, 3, and 4 increased with the progression of thyroid cancer; however, cluster 6 showed a dramatic increase during the transition from N0-tumor to N1-tumor. Furthermore, based on GO annotation, KEGG, and PPI, the crotonylated DEPs were primarily enriched in the PI3K-Akt signaling pathway, Cell cycle, and Hippo signaling pathway. Of note, crosstalk between the proteome and Kcr proteome suggested a differential changing trend, which was enriched in Thyroid hormone synthesis, Pyruvate metabolism, TCA cycle, Cell cycle, and Apoptosis pathways. Similarly, for the LNM comparison group, the DEKSs and related DEPs were primarily enriched in Hydrogen peroxide catabolic process and Tight junction pathway. Finally, according to The Cancer Genome Atlas Program (TCGA) database, the differential expression of Kcr DEPs were associated with the prognosis of thyroid cancer, indicating the prognostic significance of these proteins. Moreover, based on the clinical validation of 47 additional samples, Kcr was highly expressed in thyroid tumor tissues compared with normal tissue ($t = 9.792$, $P < 0.001$). In addition, a positive correlation was observed between Kcr and N-cadherin ($r = 0.5710$, $P = 0.0015$). Moreover, N-cadherin expression was higher in the relatively high Kcr expression group ($\chi^2 = 18.966$, $P < 0.001$).

*Correspondence:
Hui Sun
s_h@jlu.edu.cn
Nan Liang
liangnan2006@jlu.edu.cn
Full list of author information is available at the end of the article

Li *et al. Journal of Translational Medicine*   (2024) 22:874

Page 2 of 19

Conclusions Higher Kcr expression was correlated with thyroid tumorigenesis and lymphatic metastasis, which may regulate thyroid cancer progression by Pyruvate metabolism, TCA cycle, Cell cycle, and other pathways.

Keywords Crotonylation, Tumorigenesis, Lymphatic metastasis, Papillary thyroid cancer

Introduction

Thyroid cancer is one of the most common endocrine cancers, and 90% of cases are classified as papillary thyroid cancer (PTC) [1, 2]. Despite its low morbidity and mortality rates, the incidence of thyroid cancer has been increasing annually worldwide. Lymph node metastasis is one of the malignant characteristics of thyroid cancer, and recurrence indicates poor prognosis. Currently, given the unknown molecular mechanisms underlying thyroid cancer development and progression, identifying putative mechanisms in this cancer is necessary to facilitate the development of new treatments.

Post-translational modification (PTM) of proteins plays an important role in many biological processes and disease development [3, 4]. It is involved in gene regulation, material metabolism, embryonic development, and other processes. To date, more than 400 types of PTM have been discovered [5–7]. In addition to classic acetylation modifications, a batch of emerging short-chain lysine acylation reactions have been identified, including 2-hydroxyisobutyrylation, succinylation, and crotonylation [8–11]. Lysine crotonylation (Kcr) refers to the transfer of crotonyl groups to lysine residues catalyzed by crotonyl transferase. It is structurally similar to acetylation in that crotonylation contains one more C–C double bond than acetylation, which results in its unique biological function. Most studies on Kcr have focused on histones, whose functions primarily involve embryonic development, disease prevention, and gene expression. Until 2017, nonhistone Kcr had been increasingly identified [12], and it is associated with tumor progression, aging, and myocardial ischemia–reperfusion [13–15]. However, our current understanding of Kcr is incomplete and requires further study. In particular, the possible functions and mechanisms of Kcr during the development and progression of thyroid cancer are not well understood.

In this study, we established a crotonylated proteomic profile in thyroid cancer and describe the molecular changes that occur during its development and progression. We hope to gain insight into the molecular mechanisms of PTM from a novel perspective.

Materials and methods

Samples collection

All samples were from the department of Thyroid surgery, China-Japan Union hospital of Jilin University. Patients with PTC who had undergone surgical treatment and pathologically confirmed were included in the study. Tumor samples and normal samples next to cancer were collected 30 min after surgery, immediately transferred to sterilized vials, frozen with liquid nitrogen, and stored at − 80 °C. The validation samples were collected from the pathology department, along with information on their clinicopathological characteristics.

Ethical standards

This study was conducted in accordance with the Declaration of Helsinki (2013 revision). All sampling procedures were approved by the Institutional Review Committee of China-Japan Union hospital of Jilin University (No.20220804014). All patients signed the informed consent.

Protein extraction

The sample was removed from − 80 °C, an appropriate amount of tissue sample was weighed into a liquid nitrogen pre-cooled mortar, and liquid nitrogen was added and fully ground to powder. Each group of samples was sonically lysed by adding powder $4 \times$ volume lysis buffer (8 M urea, 1% protease inhibitor, 3 μM TSA, 50 mM NAM, and 2 mM EDTA). Centrifuge at 12,000 g at 4 °C for 10 min, remove cell debris, transfer the supernatant to a new centrifuge tube, and perform protein concentration determination using BCA kit.

Trypsin digestion

Dithiothreitol was added to the protein solution to make it a final concentration of 5 mM and reduced at 56 °C for 30 min. Acetamide iodoacetamide was then added to the final concentration of 11 mM and incubated at room temperature in the dark for 15 min. Finally, dilute the urea concentration of the sample to less than 2 M. Add pancreatic enzyme at a mass ratio of 1:50 (trypsin: protein) and hydrolyze overnight at 37 °C. Add pancreatic enzyme at a mass ratio

Li *et al. Journal of Translational Medicine*   (2024) 22:874

Page 3 of 19

of 1:100 (pancreatin: protein) and continue enzymatic hydrolysis for 4 h. Affinity enrichment of crotonylated polypeptides.

TMT labeling

Tryptic peptides were firstly dissolved in 0.5 M TEAB. Each channel of peptide was labeled with their respective TMT reagent (based on manufacturer's protocol, Thermo Scientific), and incubated for 2 h at room temperature. Five microliters of each sample were pooled, desalted and analyzed by MS to check labeling efficiency. After labeling efficiency check, samples were quenched by adding 5% hydroxylamine. The pooled samples were then desalted with Strata X SPE column (Phenomenex) and dried by vacuum centrifugation.

Pan antibody-based PTM enrichment

To enrich modified peptides, tryptic peptides dissolved in NETN buffer (100 mM NaCl, 1 mM EDTA, 50 mM Tris–HCl, 0.5% NP-40, pH 8.0) were incubated with pre-washed antibody beads (PTM-503, PTM Bio) at 4 °C overnight with gentle shaking. Then the beads were washed for four times with NETN buffer and twice with H2O. The bound peptides were eluted from the beads with 0.1% trifluoroacetic acid. Finally, the eluted fractions were combined and vacuum-dried. For LC–MS/MS analysis, the resulting peptides were desalted with C18 ZipTips (Millipore) according to the manufacturer's instructions。

LC–MS/MS analysis

Peptides were dissolved by liquid chromatography mobile phase A and separated using an EASY-nLC 1200 Ultra performance liquid system. The mobile phase A was an aqueous solution containing 0.1% formic acid and 2% acetonitrile. Mobile phase B was an aqueous solution containing 0.1% formic acid and 90% acetonitrile. Liquid phase gradient Settings: $0 \sim 38$ min, 9–25% B; 38–52 min, 25–35% B; 52–56 min, 35–80% B; The flow rate was maintained at 400 nL/min at 80% B for 56 to 60 min.

Peptides by ultra high performance liquid separation system are put into the NSI of ionization ion source and then into Q Exactive HF-X mass spectrometry analysis. Ion source voltage is set to 2.0 kV, peptides mother ion and its secondary debris are using high-resolution Orbitrap detection and analysis. The scanning range of the primary mass spectrometry was set to 350–1600 m/z, and the scanning resolution was set to 120,000. The scanning range of secondary mass spectrometry was fixed at 100 m/z, and the secondary scanning resolution was set at 30,000. The data acquisition mode used data-dependent scanning (DDA) program, that is, after the primary scanning, the top 20 peptide parent ions with the highest

signal intensity were selected to enter the HCD collision cell for fragmentation with 28% fragmentation energy, and the secondary mass spectrometry analysis was also performed in turn. In order to improve the effective utilization of mass spectrometry, the automatic gain control (AGC) was set to 1E5, the signal threshold was set to 5E4, the maximum injection time was set to 100 ms, and the dynamic exclusion time of tandem mass spectrometry scanning was set to 15 s to avoid repeated scanning of parent ions.

Database search

The resulting MS/MS data were processed using Max-Quant search engine (v.1.5.2.8). Tandem mass spectra were searched against the human SwissProt database (20317entries) concatenated with reverse decoy database. Trypsin/P was specified as cleavage enzyme allowing up to 4 missing cleavages. The mass tolerance for precursor ions was set as 20 ppm in First search and 5 ppm in Main search, and the mass tolerance for fragment ions was set as 0.02 Da. Carbamidomethyl on Cys was specified as fixed modification. Acetylation on protein N-terminal, oxidation on Met, crotonylation on Lys were specified as variable modifications. TMT-10plex quantification was performed. FDR was adjusted to < 1% and minimum score for peptides was set > 40.

Motif analysis

Mo Mo (motif-x algorithm) software was used to label sequence patterns around Kcr in all crotonylated protein sequences and sequence that modified amino acid composition at specific locations in 21mer (10 amino acids upstream and downstream of the site). All different database protein sequences as background database parameters. The minimum number of modifications is set to 20. Mark the original motif—x for the simulation, and the other parameters are set to default. Use the R-based heatmap package to generate heat maps for mold analysis.

Mfuzz

Sites identified from DEPs by likelihood ratio test (adjusted P value < 0.05), c-means clustering using R-wrap Mfuzz to characterize dynamic changes in expression patterns. Fuzzy C-means clustering is a soft clustering method that uses the Mfuzz algorithm with two key parameters. The algorithm iteratively assigns the profile to the cluster with the shortest Euclidean distance while minimizing the arbitrary objective function.

Subcellular localization

Subcellular localization of eukaryotic cells was predicted using Wolfpsort PSORT II, a software for predicting subcellular localization of eukaryotic cells.

Li *et al. Journal of Translational Medicine*   (2024) 22:874

Page 4 of 19

KEGG pathway annotation

KEGG is an information network that connects known molecular interactions, such as metabolic pathways, complexes, and biochemical reactions. KEGG pathways mainly include: metabolism, genetic information processing, environmental information processing, cellular processes, human diseases, drug development, etc. Firstly, using KEGG online service tools KAAS to annotated protein's KEGG database description. Then mapping the annotation result on the KEGG pathway database using KEGG online service tools KEGG mapper.

GO annotation

Gene Ontology (GO), is an important bioinformatics analysis method and tool for expressing various properties of genes and gene products. GO annotations are divided in 3 broad categories: Biological Process, Cellular Component, and Molecular Function, which explain the biological role of proteins from different perspectives. We statistically performed statistics on the distribution of differentially expressed proteins in GO secondary annotations.

PPI network analysis

The differential protein database numbers or protein sequences screened in different comparison groups were compared with the STRING (v.10.5) protein network interaction database, and the relationship was extracted according to the confidence score > 0.7 (high confidence). The differential protein interaction network was then visualized through the R package "networkD3" tool.

Immunohistochemistry staining

The para-cancerous and PTC tissues were sectioned, fixed in 4% paraformaldehyde, embedded in paraffin, and cut into sections with a thickness of 6 μm. To enhance antigen exposure and deactivate endogenous peroxidase activity, the sections were deparaffinized, rehydrated, and treated with Tris–EDTA buffer. Subsequently, the slices underwent boiling in a pressure cooker for 5 min. After three washes, the sections were incubated with BSA for 30 min followed by overnight incubation with antibodies at 4 ℃. On day two, secondary antibodies were applied to the sections for 1 h at room temperature. Finally, the sections were stained with hematoxylin, dehydrated, and fixed using neutral resin.

Statistics

Standard bilateral Student's t test (paired) was used for pairwise comparison, and X^2 test was used to evaluate the relationship between Kcr expression and clinicopathological features. All statistical analyses were performed using Graph Pad Prism 8, and $p < 0.05$ was considered statistically significant.

Results

Comprehensive landscape of Kcr DEPs and DEKSs in thyroid cancer

To examine the characteristics of protein crotonylation in thyroid carcinoma, six pairs of thyroid carcinoma and adjacent tissue were collected and further subjected to TMT-labeled LC–MS/MS (Fig. 1a). The 12 specimens were divided into N0 and N1 groups based on the presence or absence of lymph node metastasis. The N0 group did not present with lymph node metastasis, whereas the N1 group was diagnosed with lymph node metastasis. We focused on two comparisons: (1) the difference in Kcr between the tumor and normal groups (tumor/normal comparison group) and (2) the difference in Kcr between the proteomes associated with the LNM comparison groups, with the following three comparisons: standardized N1 tumor vs. normal/N0 tumor vs. normal group, N1 tumor/N0 tumor group, and differences between N1 tumor/N1 normal and N0 tumor/N0 normal. The heat map generated by Pearson correlation coefficient revealed consistency among the six pairs of specimens (Fig. 1b). Using a fold-change threshold of > 1.3 or < 0.67, 262 proteins and 702 crotonylation sites were quantified in the Kcr proteome, whereas 5203 proteins were quantified in the proteome (Fig. 1c). As shown in Fig. 1d, for the tumor/normal comparison group, 110 differentially expressed Kcr sites (DEKSs) of 57 DEPs were upregulated, whereas 59 DEKSs of 43 DEPs were downregulated; however, only approximately 20 DEKSs and DEPs were differentially regulated in the LNM comparison group. In addition, in the tumor/normal comparison group, 72.34% of the DEPs were associated with only one DEKS, whereas 15.96% were associated with two DEKSs (Fig. 1e). Similarly, > 83.33% of the DEPs were associated with only one DEKS in the LNM comparison group.

Changes in the characteristics of DEKSs during thyroid tumorigenesis

To establish a Kcr proteomic profile for thyroid cancer development, the MoMo tool was used to analyze the motif characteristics of crotonylated sites within the tumor/normal comparison group (Fig. 2a). The heatmap reflected peptide sequences consisting of 10 amino acids upstream and downstream of the identified modification sites. The frequency of lysine (K) residues was high at positions 5 and 6. Alanine(A) residues occurred more frequently at positions − 4, − 5, and 2, 3. Glutamate (E) residues were more likely to be found at position − 2. In contrast, the frequency of cysteine (C) and proline
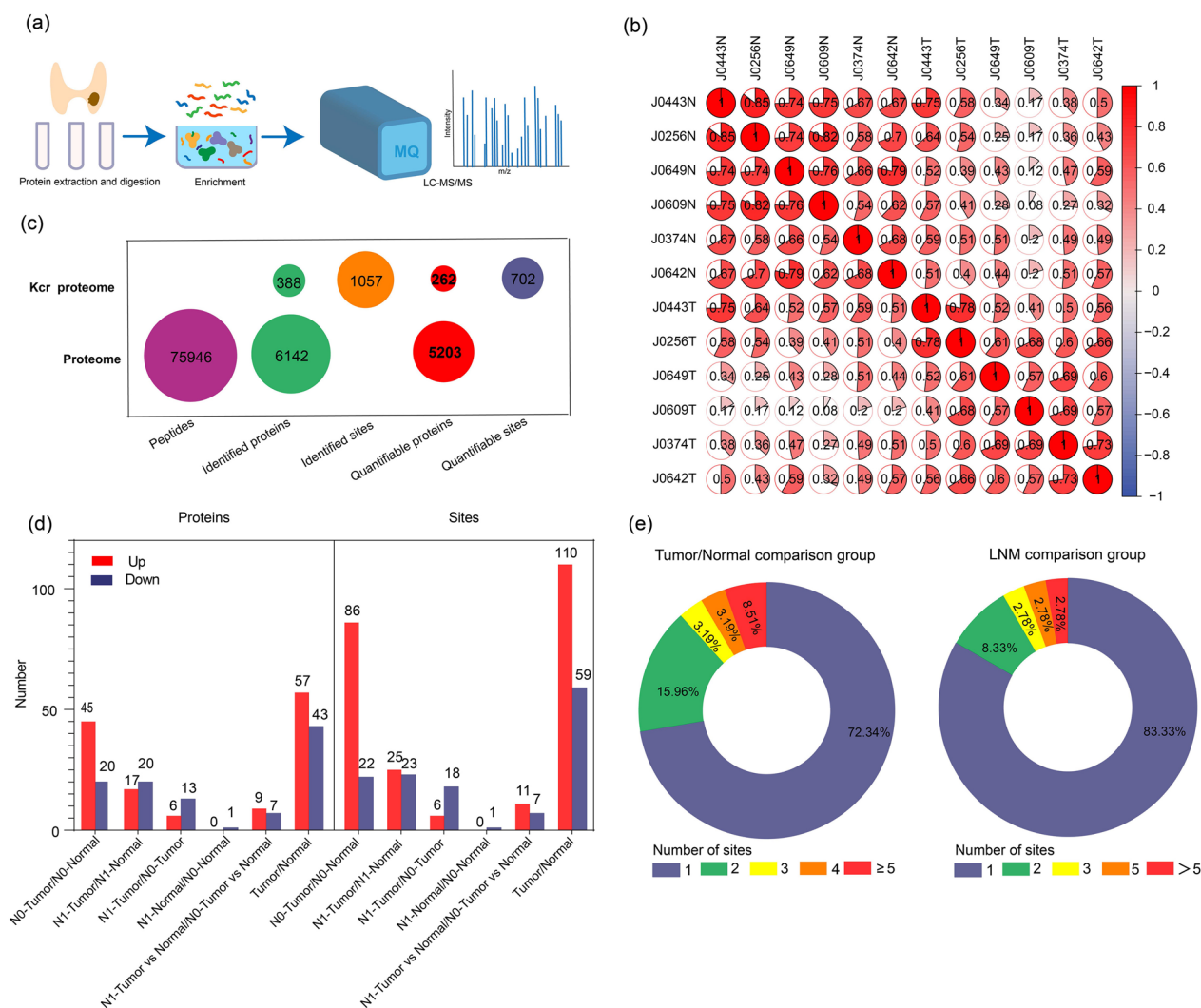
Fig. 1 Comprehensive landscape of Kcr in thyroid cancer tissues and adjacent tissues. **a** Schematic diagram of the workflow of the study. **b** Heatmap of Pearson correlation coefficients from all quantified proteins between each pair of samples. **c** The bubble chart showed the number of Kcr-modified peptides, Kcr sites, and proteins identified by MS. **d** Overview of Kcr proteins and sites. Blue indicated down-regulated proteins or sites, and red indicated up-regulated proteins or sites. **e** Statistics on the number of Kcr sites on DEPs in the Tumor/Normal comparison group and LNM comparison group

(P) residues was low. Furthermore, by analyzing the frequency of specific crotonylation sites on lysine residues, three conserved motifs were identified: xxxxxxxxEx_K_ xxxxxxxxxx and xxxxxxAxxx_K_xxxxxxxxxx were the top two motif logos. The top 10 upregulated and downregulated DEKSs were listed in Fig. 2b. Hook Microtubule Tethering Protein 3 (HOOK3)-K655, Hemoglobin Subunit Alpha (HBA1)-K17, and Hemoglobin Subunit Delta (HBD)-K18 were upregulated. Plectin (PLEC)-K1626, Actinin Alpha 1 (ACTN1)-K312, Heat Shock Protein 90 Alpha Family Class A Member 1 (HSP90AA1)-K632 were downregulated. Based on a domain enrichment analysis (Supplement Fig. 1a and b), some upregulated DEKSS

were significantly enriched in the 14–3-3 domain, Heat shock protein Hsp90, N-terminal domain, and Histidine kinase-like ATPase, C-terminal domain. Downregulated sites were primarily identified in Lamin Tail Domain.

To study the dynamic expression patterns of upregulated DEKSs during thyroid tumorigenesis, Mfuzz software was used to divide the 110 sites of the tumor/normal comparison group into 6 modules (Fig. 2c). The sites were classified into three groups as follows: normal group (N0 normal and N1 normal), tumor without lymph node metastasis group (N0-Tumor), and tumor with lymph node metastasis group (N1-Tumor). The expression patterns of clusters 1, 3, and 4 gradually increased during
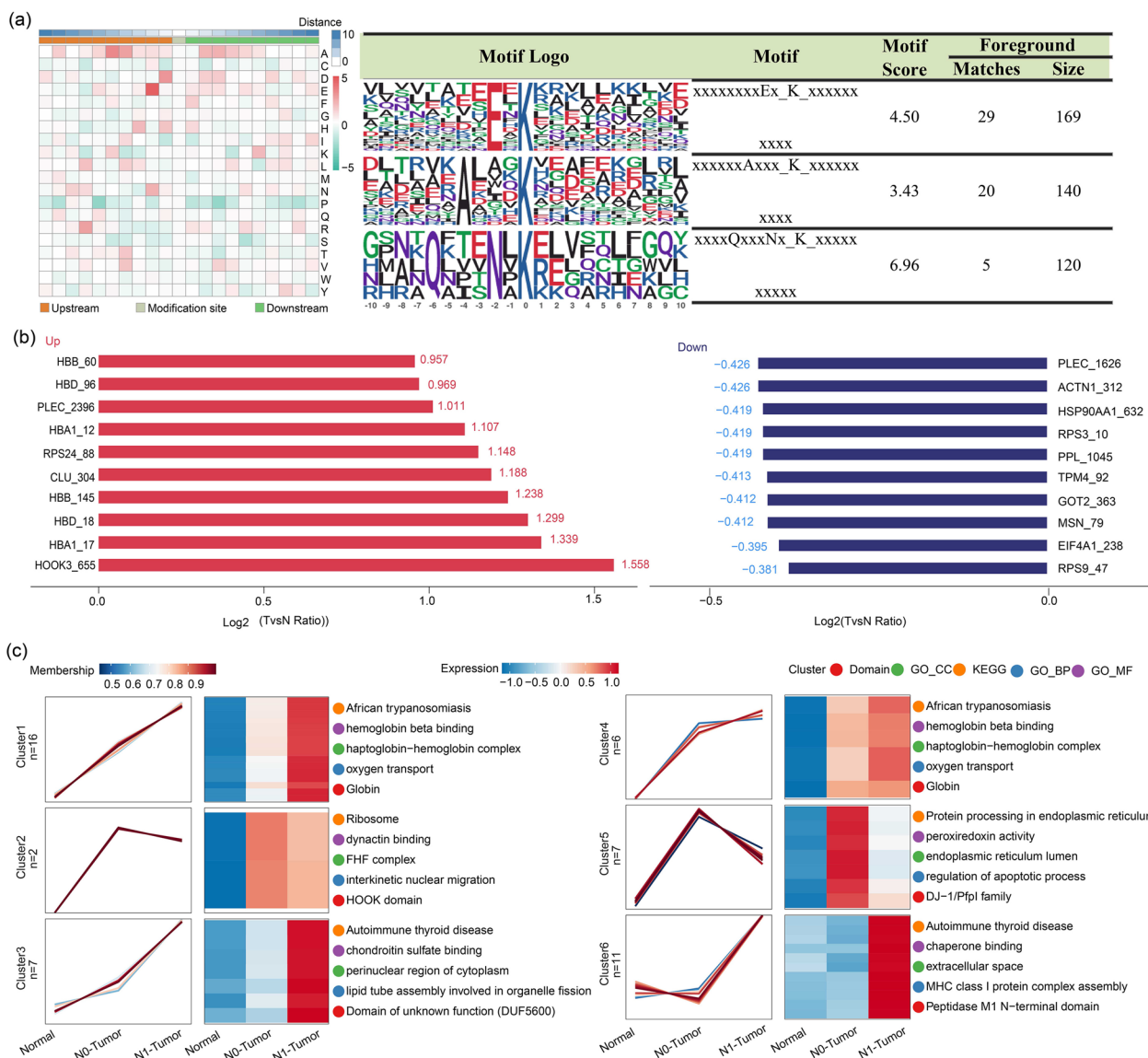
Li *et al. Journal of Translational Medicine*   (2024) 22:874

Page 6 of 19

Fig. 2 Characteristics and expression pattern clustering of DEKSs. **a** Heat map of amino acid occurrence frequency enrichment near modification sites. The frequency significance of each amino acid at a specific location was calculated by the enrichment test method, and then the heat map was drawn after log10 conversion of the p value. The different colors in the figure showed the frequency changes of each amino acid at the specified position to reflect the characteristics of Motif. Red indicates high frequency and green indicated low frequency. Motif feature logo diagram. When a feature sequence contained a number of identified modification sites greater than 20, and the statistical test p-value was less than 1e-6, the feature sequence was considered to be a motif of the modified peptide. Motif characteristics were reflected in the height ratio of amino acid abbreviations at specific locations. **b** Peptides with differences in crotonylation in the Tumor vs Normal group. Blue represented peptides that were downregulated in cancerous tissue, and red represented peptides that were upregulated in cancerous tissue. The name of the gene described in the peptide has been marked in each bar. **c** Continuous sample expression pattern clustering result plot. 6 clusters were identified using Mfuzz software. The Kcr proteins in Cluster 1, Cluster 3 and Cluster 4 showed a consistent upward trend from normal tissue to N1-Tumor, representing the process of thyroid cancer. The Kcr proteins in Cluster 2 and Cluster 5 showed a downward trend from N0-Tumor to N1-Tumor, while Cluster 6 showed an upward trend, suggesting the development of thyroid cancer

the progression of thyroid cancer. These sites were significantly enriched for African trypanosomiasis, Autoimmune thyroid disease, hemoglobin beta binding, and the haptoglobin–hemoglobin complex. Of note, a dramatic

increase was observed in cluster 6 during the transition from N0-tumor to N1-tumor, although no change was evident from normal to tumor. These Kcr sites appeared to be particularly associated with lymph node metastasis

Li *et al. Journal of Translational Medicine*   (2024) 22:874

Page 7 of 19

and were enriched in Autoimmune thyroid disease, chaperone binding, and extracellular space. Clusters 2 and 5 were initially upregulated during the transition from normal to tumor but later downregulated during the transition from N0-tumor to N1-tumor. These related DEKS were primarily enriched in Ribosome, dynactin binding, Autoimmune thyroid disease, and chondroitin sulfate binding. These findings suggested that these DEKSs, and their associated signaling pathways, may play important roles in the development of thyroid cancer.

Potential functions and molecular mechanisms of crotonylated DEPs in thyroid tumorigenesis

To further explore the potential functions and mechanisms of Kcr modification in thyroid tumorigenesis, we analyzed crotonylated DEPs in the tumor/normal comparison group. A volcano map revealed that 110 sites in 57 proteins were upregulated and 59 sites in 43 proteins were downregulated (Fig. 3a). Based on subcellular localization analysis (Fig. 3b), nearly half of the crotonylated DEPs were located in the cytoplasm. Interestingly, 17.5% (16 out of 91) were located in the mitochondria, which may be associated with cancer metabolism. In addition, Go annotation was applied to the upregulated and downregulated DEPs separately, which included biological process (BP), cellular component (CC), and molecular function (MF) (Fig. 3c). Both upregulated and downregulated DEPs were primarily enriched in cellular processes, biological regulation, metabolic processes, binding, catalytic activity, and structural molecule activity. As shown in the clusters of the COG/KOG category analysis (Fig. 3d), the upregulated crotonylated DEPs were emphatically clustered in posttranslational modification, protein turnover, chaperones, energy production and conversion, and the cytoskeleton. For downregulated crotonylated DEPs, translation, ribosomal structure and biogenesis, cytoskeletal activity, and energy production, and conversion were primarily associated.

To gain insight into the putative molecular mechanisms underlying the tumorigenesis of crotonylated DEPs, KEGG analysis was performed (Fig. 4a). Upregulated DEPs were primarily enriched in protein processing in the endoplasmic reticulum, antigen processing and presentation, thyroid hormone synthesis, and the hippo signaling pathway. Downregulated DEPs were primarily involved in the regulation of actin cytoskeleton, cysteine and methionine metabolism, and pyruvate metabolism. In addition, according to the PPI network (Fig. 4b), all upregulated crotonylated DEPs were primarily enriched in the PI3K-Akt signaling pathway, Cell cycle, and Hippo signaling pathways. These results suggested that Kcr modification may regulate thyroid tumorigenesis through these pathways.

Crosstalk of the proteome and Kcr proteome in thyroid tumorigenesis

To further examine the crosstalk between the proteome and Kcr proteome, as well as its roles in thyroid tumorigenesis, we analyzed the DEKSs and DEPs together. Based on a nine-quadrant map (Fig. 5a), five proteins and five Kcr sites were upregulated simultaneously, including lamin A/C (LMNA)-K417, Pyruvate Kinase M1/2 (PKM)-K135, and Diablo IAP-Binding Mitochondrial Protein (DIABLO)-K146. Of note, in the first quadrant, 28 proteins were downregulated, whereas 94 Kcr sites were upregulated, such as HBA1-K17, HBD-K18, and HBA1-K145. In contrast, in the ninth quadrant, 44 proteins were upregulated, and 70 Kcr sites were downregulated, including LMNA-K450, Cytochrome C Oxidase Subunit 5A (COX5A)-K115, and Solute Carrier Family 25 Member 6 (SLC25A6)-K147. We assumed that differential changes between the DEPs and DEKSs levels could be interesting. Some top changed and interesting DEKSs and associated DEPs were listed in Fig. 5b, such as HOOK3-K655, HBA1-K17, and PLEC-K2396.

According to cluster analysis of the KEGG pathways of crotonylated DEPs between different comparison groups (Supplement Fig. 2), we merged representative DEKSs and DEPs into enriched signaling pathways (Fig. 5c). The crotonylated proteins were primarily enriched in Thyroid hormone synthesis, Pyruvate metabolism, TCA cycle, Cell cycle and Apoptosis pathways. For the Thyroid hormone synthesis pathway, the expression of Thyroglobulin (TG) at the protein and crotonylation levels was reversed. For the Pyruvate metabolism pathway, PKM protein and its crotonylation expression levels were upregulated simultaneously, whereas Lactate Dehydrogenase A (LDHA), Aldehyde Dehydrogenase 9 Family Member A1 (ALDH9A1), and Malate Dehydrogenase 2 (MDH2) exhibited opposite changes in protein and crotonylation expression levels. In the TCA cycle, the protein levels of several key enzymes, such as MDH2 and Oxoglutarate (OGDH) were significantly increased, whereas their crotonylation levels were decreased. This suggested that crotonylation levels may affect the expression of proteins related to metabolism, and the specific mechanism warrants further study. In addition, for the Cell cycle pathway, most 14–3-3 family proteins were upregulated at the protein and crotonylation levels; however, the 3-Monooxygenase/Tryptophan 5-Monooxygenase Activation Protein Epsilon (YWHAE) protein levels was downregulated, whereas its crotonylation levels was upregulated. These data suggested that differentially changing models and profiles should be considered when determining the mechanisms responsible for the development and progression of thyroid cancer.
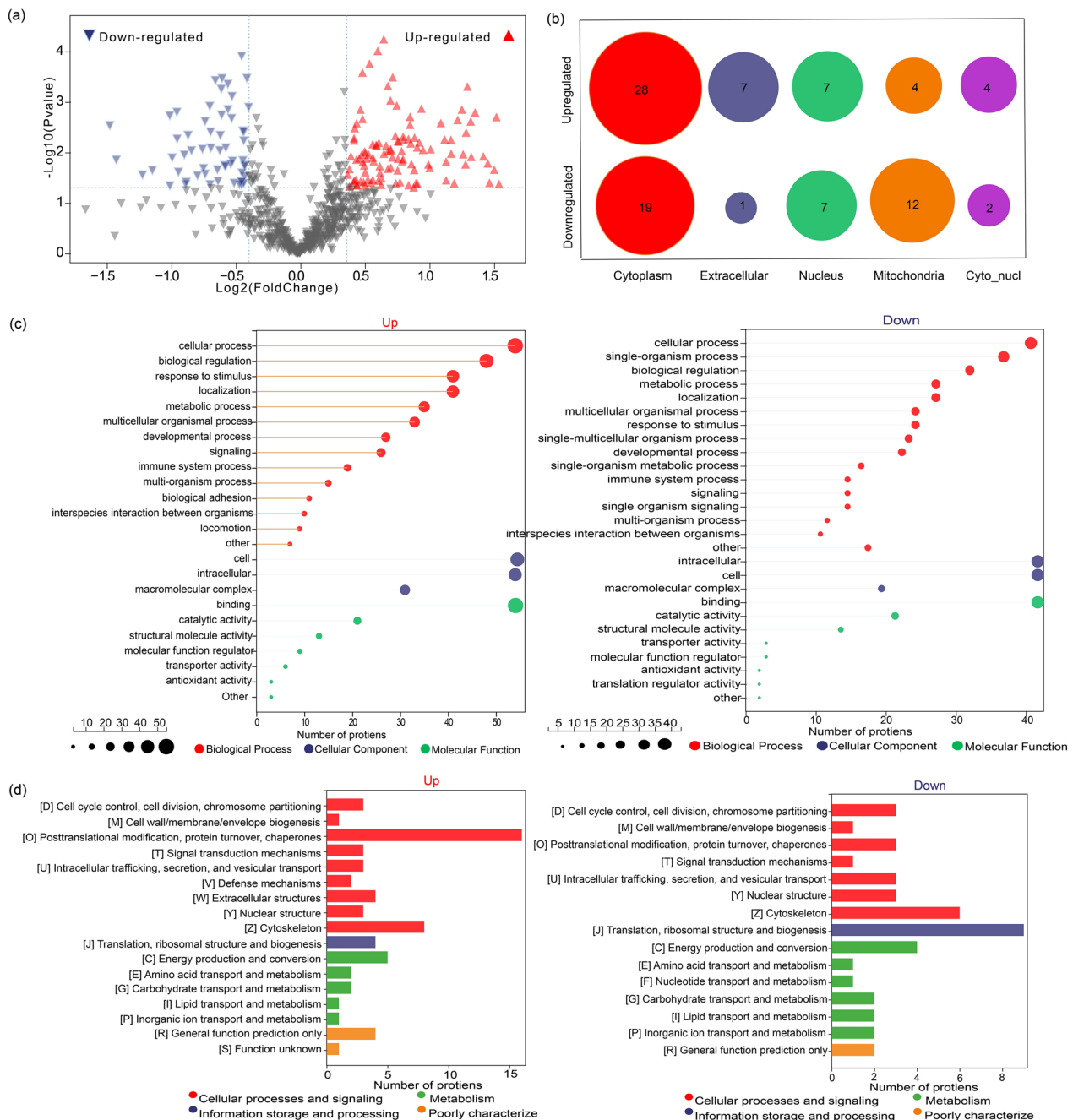
Fig. 3 Functional classification and annotation of crotonylated DEPs in thyroid cancer. **a** Volcano plots showed differences in crotonylation sites in the Tumor/Normal comparison group. **b** Subcellular localization distribution of DEPs. **c** Lollipop plot of DEPs GO secondary functional classification. **d** DEPs COG/KOG functional classification bar chart

Features and possible molecular mechanisms of the Kcr proteome in lymphatic metastasis of PTC

To determine the possible functions and molecular mechanisms of the Kcr proteome in the process of lymphatic metastasis of PTC, we specifically focused on the DEKSs and DEPs within the LNM comparison group.

As shown in Fig. 6a, the frequency of lysine (K) residue was high at position 9. Alanine(A) residues were more inclined to be distributed in positions -3, -5, and -6. Nevertheless, cysteine (C) and glycine (G) occurred rarely. Moreover, two sequences with specific crotonylation sites were discovered:
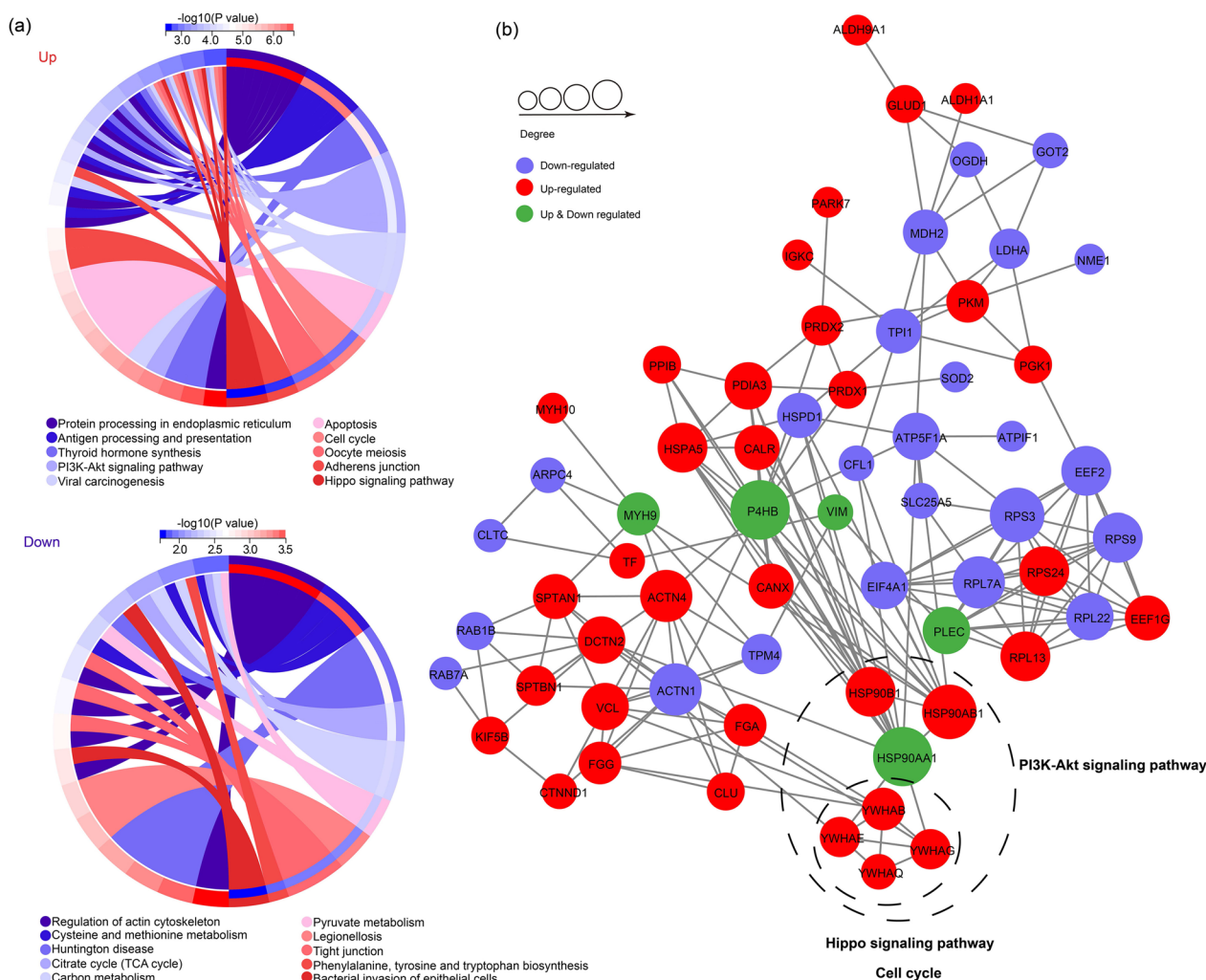
Li *et al. Journal of Translational Medicine*   (2024) 22:874

Page 9 of 19

Fig. 4 KEGG and PPI of Kcr DEPs in thyroid cancer. **a** Significant enrichment of KEGG pathway chord diagram. The pie chart above showed the first 10 pathways enriched by upregulated DEPs, and the pie chart below showed the enrichment of the first 10 pathways of downregulated DEPs. **b** DEPs interaction network diagram. The red node represented the up-regulated DEPs, the blue node represented the down-regulated DEPs, and the green node refered to the up-regulated and down-regulated DEPs. The size of the dots represented the number of interacting proteins

xxxxxAxxxx_K_xxxxxxxxxx and xxxxxxxAxx_K_xxxxxxxxxx. Subsequently, expression pattern clustering analysis was performed on 36 upregulated DEKSs (Fig. 6b). All clusters showed a significant upward trend during thyroid cancer progression. These DEKSs were primarily gathered in Complement and coagulation cascades, Autoimmune thyroid disease, and iodide transport. According to the PPI network from the LNM comparison group (Fig. 6c), the upregulated DEPs were enriched into Hydrogen peroxide catabolic process and Tight junction pathway. This suggested that lymph node metastasis of thyroid cancer may be related to crotonylation modification in these pathways.

Prognositic prediction of Kcr DEPs in thyroid cancer

To verify the predictive value of crotonylated proteins in the development and progression of thyroid cancer, TCGA database analysis was performed. According to the screening criteria, survival analysis was performed on 18 crotonylated DEPs, and 6 of them showed a potential predictive value. As shown in Fig. 7a, compared with low HOOK3 expression, high HOOK3 expression was associated with decreased progression-free survival (PFS), indicating that high HOOK3 expression was positively correlated with worse prognosis. This phenomenon was also observed in Myosin Heavy Chain 9 (MYH9) and Tyrosine 3-Monooxygenase/Tryptophan 5-Monooxygenase Activation Protein Gamma (YWHAG). However,
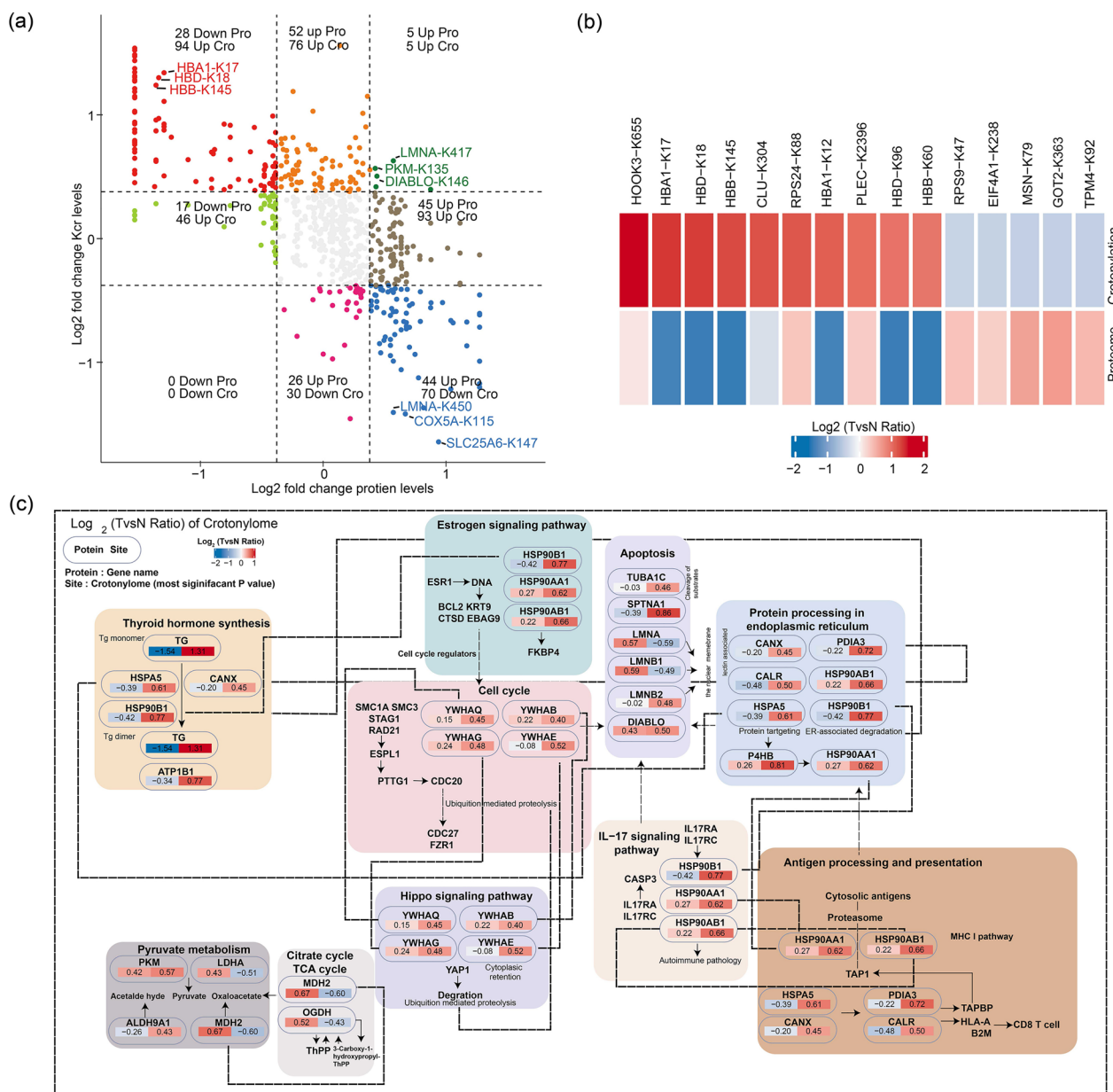
Fig. 5 Crosstalk between proteome and Kcr proteome. **a** The quadrant plot illustrated the positional changes between DEPs and DEKSs in the Tumor/Normal comparison group. Each data point represented a specific site. The x-axis and y-axis represented the tumor/normal ratio of Kcr proteome and proteome, respectively. The numbers in the corners indicated the DEPs and DEKSSs that were either upregulated or downregulated within each quadrant. Additionally, each quadrant highlighted the top three Kcr proteins and their corresponding sites. "Pro" denoted "Proteins," while "Cro" refered to "Kcr sites." **b** Comparison of changes in proteome and Kcr proteome associated with thyroid cancer. The figure shows the changes of the relative folds of the 10 sites upregulated by Kcr and the 5 sites of Kcr down-regulated in the Tumor/Normal comparison group, and also showed the relative fold changes of the corresponding proteins. **c** KEGG pathway visualization based on proteomics and croton proteomics. DEPs on the left and DEKSSs on the right. Numbers represented the tumor/normal ratio of crotonylation and proteome

different trends had emerged in Clusterin (CLU), Heat Shock Protein 90 Beta Family Member 1 (HSP90B1), and YWHAE, suggesting that low expression of CLU, HSP90B1, and YWHAE indicated poor prognosis. In addition, the differential expression of Kcr DEPs was validated, and their expression levels were higher in cancer tissues than in adjacent tissues (Fig. 7b).

The correlation between the expression of these six proteins and clinicopathological features was further evaluated. The results showed that their expression were
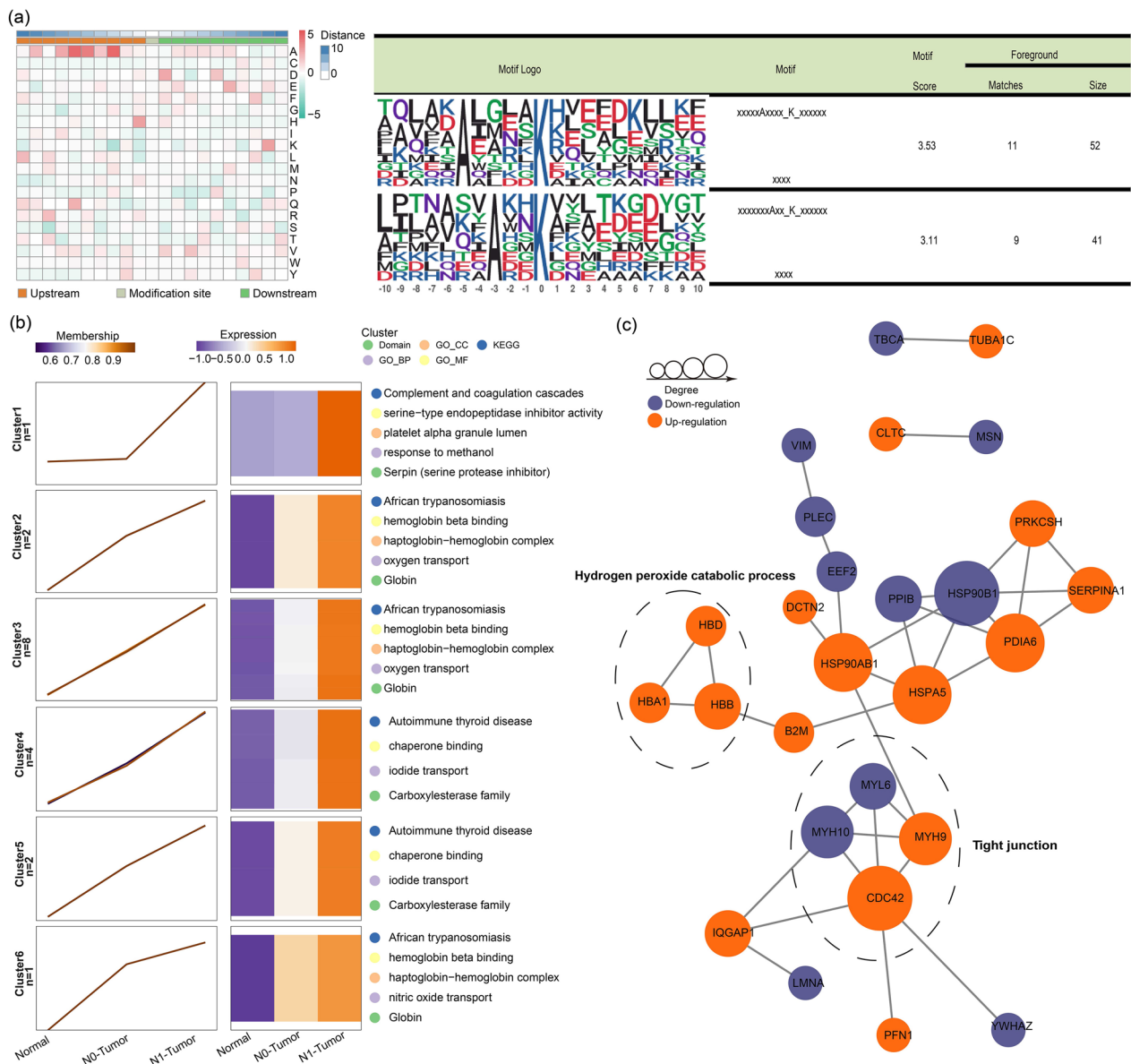
Li *et al. Journal of Translational Medicine*   (2024) 22:874

Page 11 of 19

Fig. 6 Characteristics and pathways of Kcr DEKSs in the LNM comparison group. **a** Heat map of amino acid occurrence frequency enrichment near modification sites. The frequency significance of each amino acid at a specific location was calculated by the enrichment test method, and then the heat map was drawn after log10 conversion of the p value. The different colors in the figure showed the frequency changes of each amino acid at the specified position to reflect the characteristics of Motif. Red indicated high frequency and green indicates low frequency. Motif feature logo diagram. When a feature sequence contains a number of identified modification sites greater than 20, and the statistical test p-value is less than 1e-6, the feature sequence is considered to be a motif of the modified peptide. Motif characteristics are reflected in the height ratio of amino acid abbreviations at specific locations. **b** Continuous sample expression pattern clustering result plot. 6 clusters were identified using Mfuzz software. The Kcr proteins in all cluster showed a consistent upward trend from normal tissue to N1-Tumor, representing the process of thyroid cancer. **c** Differential crotonylated protein interaction network diagram. The orange node represented the up-regulated crotonylated protein, the purple node represents the down-regulated crotonylated protein. The size of the dots represented the number of interacting proteins

correlated with tumor grade, subgroup histologic type, etc. (Fig. 7c). As shown in Fig. 7d, the expressions of CLU, HSP90B1, and YWHAE were negatively correlated with the increase of riskscore, which showed they were protective factors. On the contrary, HOOK3, MYH9, and YWHAG were risk factors, with an upward trend in their expression with the increase of riskscore.

Moreover, to better predict the prognosis of thyroid cancer, a nomogram was constructed (Fig. 7e). For example, in a 42-year-old (10.74) female (0) patient with
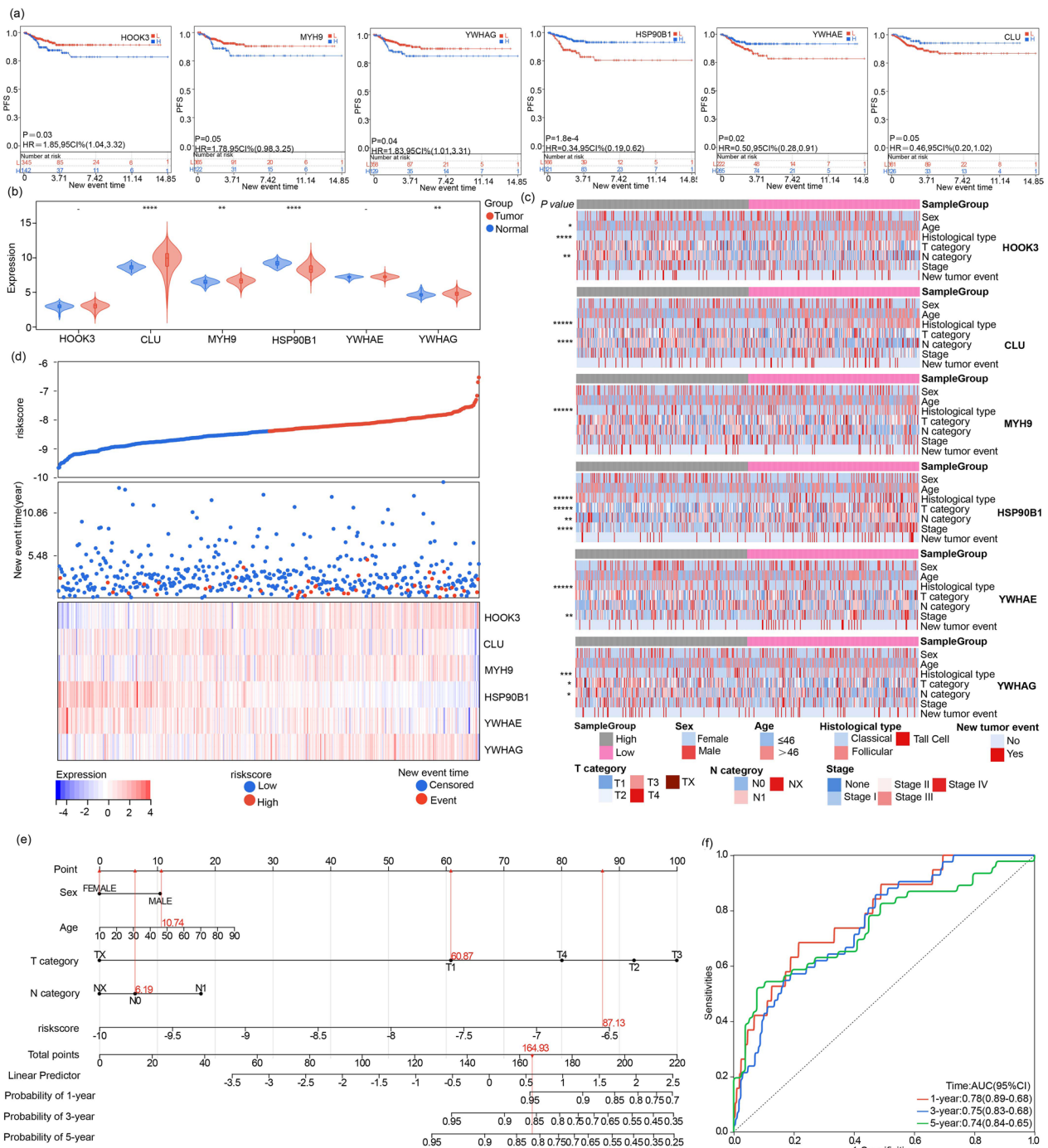
Li *et al. Journal of Translational Medicine*   (2024) 22:874

Page 12 of 19

Fig. 7 The prognositic prediction of Kcr DEPs in thyroid cancer. **a** The KM curves for PFS of 6 Kcr DEPs. **b** 6 Kcr DEPs differentially expressed in thyroid cancer, **$P < 0.01$, ****$P < 0.0001$. (**c**) Correlation between 6 DEPs expression and clinicopathological features, *$P < 0.05$, **$P < 0.01$, ***$P < 0.001$, ****$P < 0.0001$, *****$P < 0.00001$. **d** Riskscore distribution, state of each patient's prognosis, and six Kcr DEPs heat maps. **e** A nomogram was established to predict new tumor event at 1, 3, and 5 years. **f** Time-dependent ROC curves of the nomogram to predict the 1-, 3-, and 5-year progression-free surial

thyroid cancer, T1 category (60.87), N0 category (6.19), and high risk score (87.13), the score is 164.93. The 1-, 3-, and 5-year PFS rates were 95%, 86%, and 82%, respectively. The nomogram had good prediction accuracy, with a C-index of 0.72 (95% confidence interval, 0.65–0.79). The receiver operating characteristic curve

showed that the areas under the curve of the nomogram for predicting postoperative 1-, 3-, and 5-year PFS rates were 0.78, 0.75, and 0.74 (Fig. 7f). The calibration curve showed that the nomogram could predict 1-, 3-, and 5-year disease-free survival well (Supplement Fig. 3). The above validation implied that the crotonylated proteins showed good performance in predicting the prognosis of thyroid cancer.

Clinical validation of the relationship between Kcr levels and lymphatic metastasis in PTC

To further verify the differential expression of Kcr in thyroid cancer as well as the relationship between Kcr expression and PTC development, additional 47 paired PTC specimens and adjacent normal tissues were collected. Kcr expression was measured by IHC and evaluated by a pathologist. Representative images of six patients were shown in Fig. 8a. Compared with adjacent normal tissues, Kcr was significantly highly expressed in tumor tissues ($t = 9.792$, $P < 0.001$) (Fig. 8b). This result was consistent with the original sequencing data; however, inconsistent with our expectation, no significant differential expression was observed between the N0 and N1 groups ($t = 0.930$, $P = 0.357$) (Fig. 8c). This may have been the result of the smaller sample size or the lower detection efficiency. N-cadherin is a marker for the epithelial-mesenchymal transformation (EMT), which is indicative of metastasis [16]. As shown in Figs. 8d and e,
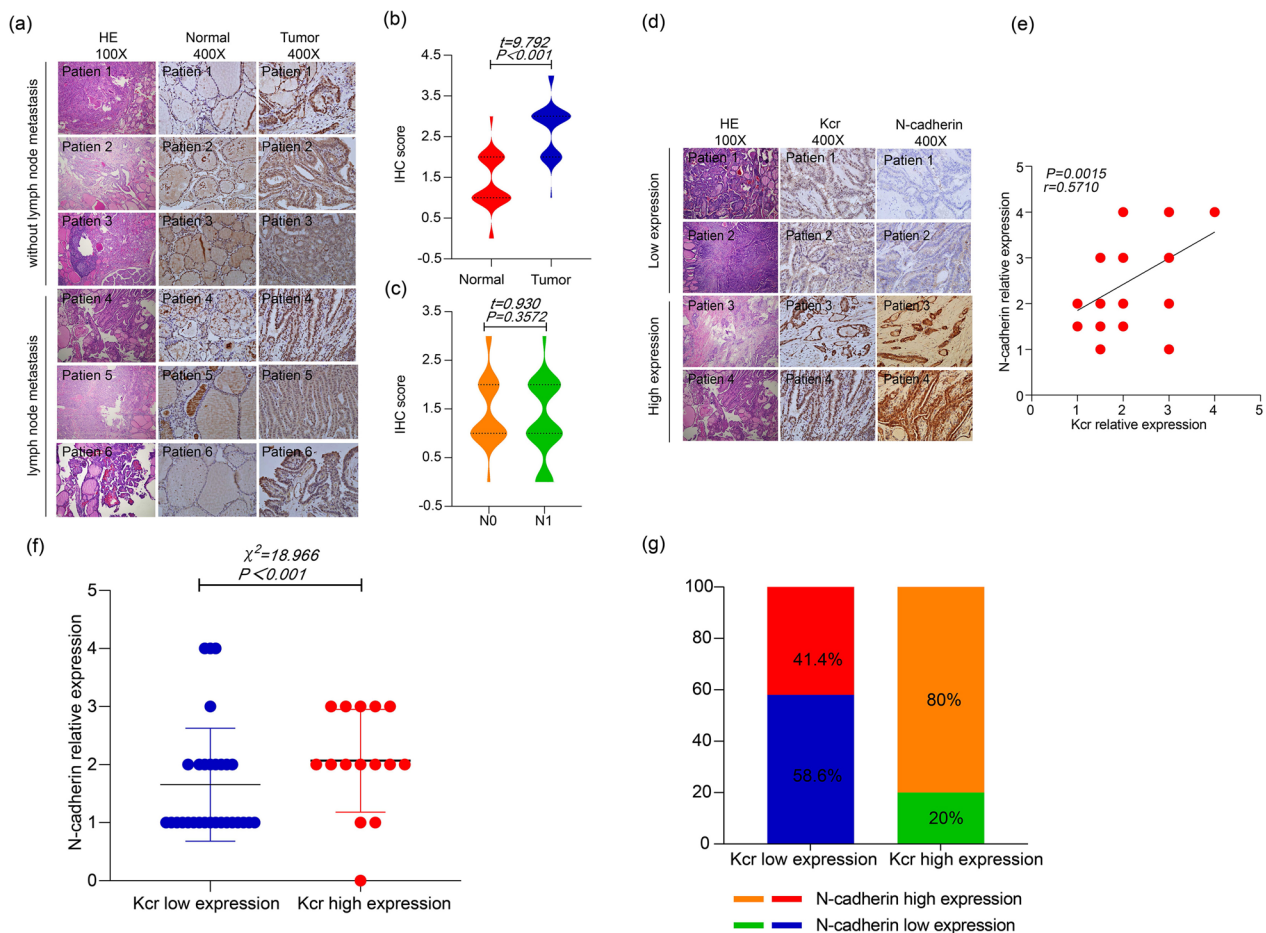

Fig. 8 Clinical validation of the relationship between Kcr with the development and progression of thyroid cancer. **a–c** Immunohistochemistry (IHC) showed that the level of crotonylation was higher in thyroid cancer tissues. However, in thyroid cancer tissues with lymph node metastasis, the level of crotonylation did not change significantly. **d, e** The Ratio of Kcr and N-cadherin IHC scores in thyroid cancer tissues of the same patient was calculated, and 12 samples that could not be calculated were excluded. The ratio ≥ 2 was defined as a relatively high expression group, otherwise a relatively low expression group. The results showed that crotonylation was positively correlated with N-cadherin. **f, g** The difference of N-cadherin IHC scores between thyroid cancer tissues and adjacent tissues of the same patient was calculated. A difference of ≥ 2 was defined as a relatively high N-cadherin expression group, otherwise a relatively low N-cadherin expression group. The results showed that most of the N-cadherin is lower expression in the Kcr low expression group

Li *et al. Journal of Translational Medicine*   (2024) 22:874

Page 14 of 19

a positive correlation between Kcr expression and N-cadherin expression was observed ($r=0.571$, $P=0.0015$), which indicated that Kcr is associated with thyroid cancer tumorigenesis and lymphatic metastasis.

We also determined whether Kcr expression was associated with clinical characteristics. We compared the IHC scores of the thyroid cancer and adjacent normal tissues of each patient. Three patients were excluded because of undetectable signals; thus, 44 tumor/normal ratios from 44 patients were obtained, with an average of 2.125. All patients were divided into a relatively high and a relatively low expression group with a ratio of 2 as the cutoff. That is, patients with a ratio > 2 were identified as the relatively high expression group, whereas those with a ratio of ≤ 2 were identified as the relatively low expression group. The statistical relationships between Kcr expression and clinical characteristics were presented in Table 1. As shown in Fig. 8f and g, the expression of N-cadherin was higher in the relatively high Kcr expression group than in the relatively low Kcr expression group ($\chi^2=18.966$, $P<0.001$), suggesting that those with high Kcr expression may be at a higher risk of developing thyroid cancer with lymphatic metastasis. However, no significant association was observed between relative

Table 1 Differences in clinical characteristics at different Kcr expression levels

Features	Relatively low expression (T/N ratio ≤ 2)	Relatively high expression (T/N ratio > 2)	χ2	p
Gender				
Male	13(44.8)	3(20.0)	0.8448	0.26
Female	16(55.2)	12(80.0)		
Age				
≤ 45	23(79.3)	8(53.3)	0.7656	0.54
> 45	6(20.7	7(46.7)		
Diameter				
≤ 1 cm	21(72.4)	9(60.0)	1.96	0.39
> 1 cm	8(27.6)	6(40.0)		
Calcification				
No	21(72.4)	10(66.7)	3.063	0.33
Yes	8(27.6)	5(33.3)		
Invasion				
No	22(75.9)	11(73.3)	3.063	0.33
Yes	7(24.1)	4(26.7)		
Thyroiditis				
No	21(72.4)	11(73.3)	5.444	0.26
Yes	8(27.6)	4(26.7)		
N-cadherin				
T-N < 2	17(58.6)	3(20.0)	18.966	< 0.001
T-N ≥ 2	12(41.4)	12(80.0)		

Kcr expression and sex, age, tumor diameter, calcification, local external invasion, or complicated inflammation. Again, the smaller validation set may be a limitation, and further trials with larger sample sizes are needed.

The literature review also revealed that HMGA1 and FN1, as EMT markers, were associated with the development and progression of thyroid cancer, and represented potential biomarkers for its diagnosis and prognosis [17, 18]. Thus, based on the TCGA database and our previous study, we further investigated the association between Kcr and HMGA1 and FN1. As illustrated in Fig. 9, the correlation between the expression of FN1 and 18 Kcr DEPs was examined. The findings indicated a significant correlation between FN1 and these DEPs. Specifically, its expression was positively correlated with the expression of HOOK3 ($P=8.4e$-25, $r=0.44$), YWHAG ($P=1.7e$-19, $r=0.39$), and MYH9 ($P=2.1e$-34, $r=0.52$), which were all identified as risk factors for thyroid cancer. Similarly, the same study on HMGA1 found that HMGA1 expression was correlated with HOOK3 ($P=4.1e$-12, $r=0.31$) and MYH9 ($P=4.9e$-12, $r=0.31$). These findings suggested a correlation between Kcr expression and HMGA1 and FN1, which are EMT markers.

Discussion

The incidence of thyroid cancer, the most common endocrine malignancy, has been increasing annually. Understanding the pathogenesis of thyroid cancer is important for improving the accuracy of diagnosis and developing strategies for individual treatment. Crotonylation is a novel acylation modification that it contributes to numerous diseases. Therefore, we examined the role of crotonylation in the mechanisms of thyroid cancer occurrence and progression. First, we performed a comprehensive analysis of crotonylation in thyroid cancer tissues. Second, we analyzed the clustering of DEKSs and their pathways. In addition, the signaling pathways involved in crotonylated DEPs were identified. Crosstalk between the proteome and Kcr proteome indicated a differential expression of DEKSs and DEPs. Finally, utilizing the TCGA database, we identified that Kcr DEPs possessed significant prognostic value. In addition, we validated the association between Kcr levels and thyroid tumorigenesis and lymph node metastasis using an additional set of 47 clinical samples.

Crotonylation is a novel PTM of proteins. Since its discovery in 2011 [19], it has been proven to play a non-negligible role in various diseases, such as kidney disease, tumors, depression, bacterial infections, and AIDS [20–27]; however, these studies have focused on histones. With the development of MS, nonhistone crotonylation modification was proposed. Since then, numerous nonhistone crotonylation modifications have been identified.

Li *et al. Journal of Translational Medicine*   (2024) 22:874
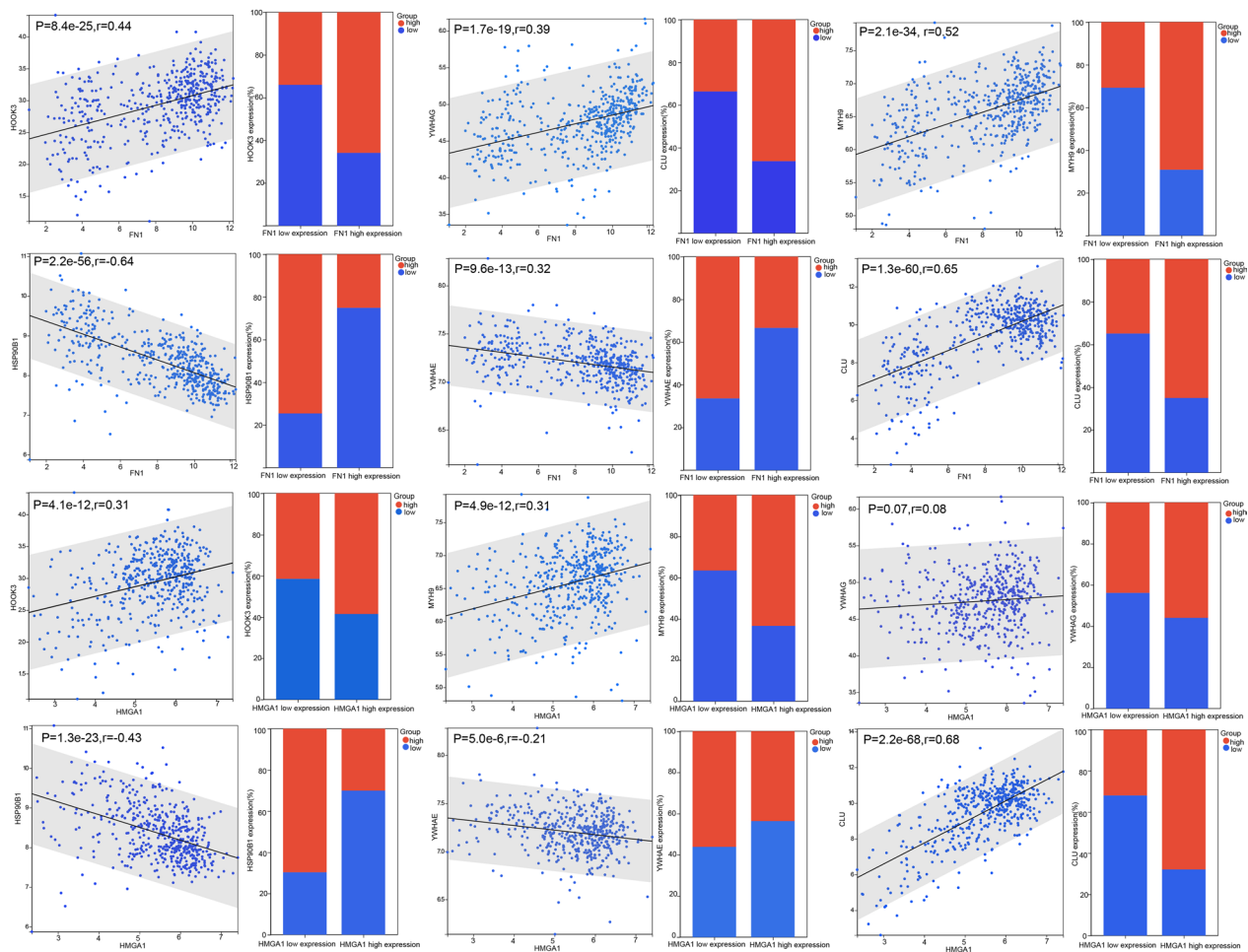
Page 15 of 19

Fig. 9 Correlation between Kcr and EMT special markers in thyroid cancer

Previous studies have shown that nonhistone crotonylation is involved in various diseases, such as kidney and cardiovascular diseases, obesity, tumors, and muscle damage [28–32, 32–34].

Crotonylation modifications are strongly associated with the pathogenesis and metastasis of some tumors. As presented in Supplementary Table 1, laminA K265/K270 crotonylation plays a crucial role in the proliferation of hepatocellular carcinoma cells [26]. High levels of crotonylation at PGD-K163 and TKT-K140 suppress the pentose phosphate pathway and glycolysis in HCC cells while constraining the Warburg effect [35]. Furthermore, Ehhadh K572cr has been implicated in promoting increased DNA damage in vitro and driving the occurrence and progression of liver cancer [27]. In cervical cancer, CDYL negatively regulates the K88, K379, and K395 sites on RPA1 and participates in the repair of DNA damage resulting from ionizing radiation or antitumor

drugs [28]. ENO1 K420cr is associated with the proliferation, invasion, and metastasis of colorectal cancer [36]. Similarly, differentially expressed Kcr sites have been identified in acute lymphoblastic leukemia [37]. This study focused on the mechanism of crotonylation in tumorigenesis and lymphatic metastasis of PTC. Based on mass spectrometry (Fig. 10), 388 Kcr proteins and 1057 Kcr sites were identified. Of these, the crotonylation of proteins, such as HOOK3, HBA1, HBD, PLEC, and ACTN1, was significantly increased in cancer tissues. In the KEGG signaling pathway analysis, these DEPs were primarily enriched in signaling pathways, such as the PI3K–Akt signaling pathway, Cell cycle, Apoptosis, TCA cycle, Pyruvate metabolism, and Hippo signaling pathways. The proteins included the 14-3-3 protein family, LMNA, TG, PKM, and LDHA. In particular, the 14-3-3 protein family has been previously implicated in cancer. In addition, LMNA, which is associated with liver

Li *et al. Journal of Translational Medicine*   (2024) 22:874

Page 16 of 19

cancer cell proliferation [30], was significantly upregulated in thyroid cancer, particularly at K417. In addition, PKM, which is highly expressed in most cancers [38], was expressed in this study. The above results indicate the involvement of crotonylation in the tumorigenesis and lymphatic metastasis of thyroid cancer.

Thyroid cancer has a 5-year survival rate of > 90% [39, 40]. Although it remains relatively benign [41], a significant concern is the possibility of lymph node metastases, which is challenging. Therefore, our next study will examine the mechanism of lymph node metastasis. First, the tissue samples were divided into non-lymph node metastasis (N0) and lymph node metastasis (N1). MS revealed that compared with the N0 group, the levels of crotonylation in corresponding proteins, such as HBD (K18), Hemoglobin Subunit Beta (HBB) (K145, K9), HBA1 (K17, K91), Peroxiredoxin 2(PRDX2) (K92), Protein Kinase C Substrate 80 K-H (PRKCSH) (K376) were significantly increased. Further analysis revealed that most of these proteins were enriched in hydrogen peroxide catabolic process and tight junction pathway. These findings present the potential involvement of crotonylation in the regulation of lymph node metastasis in thyroid cancer. Given the sample size of this study, the study must be expanded and verified. Moreover, we identified the crotonylation modification of proteins in only a small set of clinical samples, which should be verified in future in vitro and in vivo studies.

Using TCGA database, we developed a nomogram to predict prognosis with high accuracy. Among the six proteins included in the nomogram, HOOK3, MYH9, and YWHAG received particular attention because they were identified as risk factors for new tumor events following thyroid cancer surgery. HOOK3, a member of the hook microtubule-tethering protein (HOOK) family, is an adaptor protein that connects organelles to microtubules [42]. Several studies have suggested that HOOK3 is associated with cancer. For example, the RET-HOOK3 rearrangement has been reported in thyroid cancer, which is carcinogenic [43]. In another study, high HOOK3 expression levels were found to be an independent predictor of prostate cancer recurrence [44]. MYH9 is a subunit of class II conventional myosin, which interacts with actin and participates in cell movement, migration, and adhesion. MYH9 facilitates the progression of various cancers, including prostate, ovarian, esophageal, and breast cancers [45–48]. YWHAG belongs to the 14-3-3 acidic protein family, and its dysregulated expression has been observed in various cancer types, playing a crucial role in the progression of malignant tumors [49]. Thus, this nomogram can serve as a tool for predicting prognosis. Nevertheless, the accuracy of this predictive capability requires further validation in future multicenter studies with larger cohorts.

In previous studies, Kcr was considered to be more strongly expressed in cancer tissue, and we demonstrated this in thyroid cancer using IHC. In this study, Kcr expression was significantly higher in cancer tissues than in normal tissues. Although there was no significant difference between the lymph node and non-lymph node metastasis groups, there was a trend toward higher expression in the lymph node metastasis group. With respect to higher Kcr expression in the lymph node metastasis group, we examined the relationship between Kcr and metastasis. As a marker of EMT, N-cadherin exhibits increased expression and promotes cancer cell migration and invasion in various cancers [50]. Our results showed that the relative expression of Kcr was positively correlated with the expression of N-cadherin. Therefore, lymph node metastasis from thyroid cancer may be related to increased Kcr levels.

A limitation of this study is that it was a single-center study with a small sample size. Therefore, the results should be validated using a larger sample size from multiple centers. In addition, although sequencing results were provided, further experimental verification of important target molecules is required.

In summary (Fig. 10), we examined the potential functions and mechanisms of lysine crotonylation modification in the tumorigenesis and lymphatic metastasis of PTC. First, during thyroid tumorigenesis, DEKSs and crotonylated DEPs may regulate thyroid tumorigenesis through metabolism, the PI3K–Akt signaling pathway, Cell cycle, and Hippo signaling pathway. Second, the crosstalk between the proteome and Kcr proteome indicates differentially changing trends between DEPs and DEKSs levels, which might tell an interesting story and should be paid special attention. In addition, DEKSs and crotonylated DEPs may regulate lymphatic metastasis by Hydrogen peroxide catabolic process and Tight junction pathway. Finally, base on the TCGA database, we found that Kcr DEPs had significant potential for prognostic prediction. In addition, clinical validation suggested that higher Kcr expression was correlated with thyroid tumorigenesis and lymphatic metastasis. These results suggested that Kcr may play an important role in PTC development and progression, providing a theoretical basis for its future application in the clinical management of thyroid cancer.
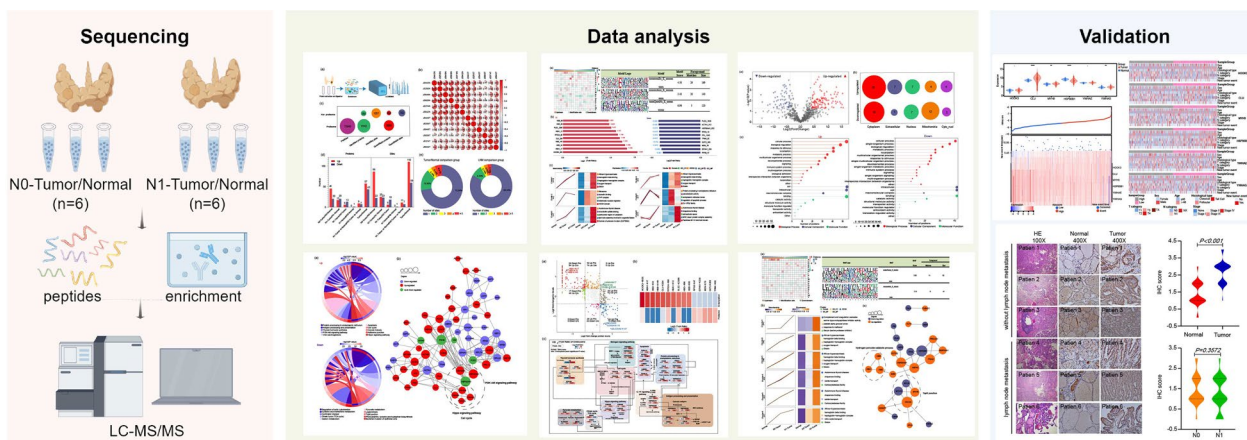
Li *et al. Journal of Translational Medicine*   (2024) 22:874

Page 17 of 19

Fig. 10 The work flow chart, by Figdraw

Abbreviations
BP	Biological process
CC	Cellular component
DEPs	Differentially expressed proteins
DEKSs	Differentially expressed Kcr sites
EMT	Epithelial-mesenchymal transformation
GO	Go Ontology
IHC	Immunohistochemistry
Kcr	Lysine crotonylation
KEGG	Kyoto Encyclopedia of Genes and Genomes
MF	Molecular function
PTC	Papillary thyroid cancer
PPI	Protein–protein interaction analysis
PTM	Post-translational modification

Supplementary Information

The online version contains supplementary material available at https://doi.org/10.1186/s12967-024-05651-4.

Supplementary file 1: Fig 1 Domain enrichment analysis.. Up-regulated DEKSs.. Down-regulated DEKSs

Supplementary file 2: Fig 2 Kcr protein KEGG enrichment pathway heatmap in all comparison groups. Red represents upregulated protein and green represents downregulated protein

Supplementary file 3: Fig 3 Calibration curves of the nomogram

Supplementary file 4: Table 1 Differences in clinical characteristics at different Kcr expression levels

Author contributions
All authors contributed to the study conception and design. Hui Sun and Nan Liang designed the study. Zhaokun Li, Jingting Li and Fang Li performed the bioinformatics analyses and statistical work. Liang Han and Nan Liang conducted experiments. Chengqiu Sui collated the original data. Le Zhou, Daqi Zhang and Yantao Fu collected clinical samples. Fang Li, Rui Du and Jiedong Kou gave instructions on how to use the new software. Hui Sun, Nan Liang and Gianlorenzo Dionigi supervised the study. Zhaokun Li drafted the manuscript. Nan Liang reviewed and revised the manuscript. Hui Sun and Nan Liang provided the funding supports. All authors read and approved the submitted manuscript.

Availability of data and materials
Some or all datasets generated and/or analyzed during the current study are not publicly available, but are available from the corresponding author upon reasonable request.

Declarations

Ethics approval and consent to participate
This study was conducted in accordance with the Declaration of Helsinki (2013 revision). All sampling procedures were approved by the Institutional Review Committee of China-Japan Union hospital of Jilin University (No.20220804014). All patients signed the informed consent.

Consent for publication
Not applicable.

Competing interests
The authors declared no competing interests.

Author details
[1]Division of Thyroid Surgery, Jilin Provincial Key Laboratory of Surgical Translational Medicine, Jilin Provincial Precision Medicine Laboratory of Molecular Biology and Translational Medicine On Differentiated Thyroid Carcinoma, The China-Japan Union Hospital of Jilin University, 126 Xiantai Street, Changchun 130033, Jilin, China. [2]Division of Pathology, The China-Japan Union Hospital of Jilin University, Changchun City, , Jilin Province, China. [3]Division of General and Endocrine Surgery, Istituto Auxologico Italiano IRCCS, Department of Medical Biotechnology and Translational Medicine, University of Milan, Milan, Italy.

References
1. Su Z, Bao W, Yang G, Liu J, Zhao B. SOX12 promotes thyroid cancer cell proliferation and invasion by regulating the expression of POU2F1 and POU3F1. Yonsei Med J. 2022;63:591.

Li *et al. Journal of Translational Medicine*   (2024) 22:874

Page 18 of 19

2. Kang IK, Kim K, Park J, Bae JS, Kim JS. Central lymph node ratio predicts recurrence in patients with N1b papillary thyroid carcinoma. Cancers. 2022;14:3677.

3. Hu Y, Pan J, Shah P, Ao M, Thomas SN, Liu Y, et al. Integrated proteomic and glycoproteomic characterization of human high-grade serous ovarian carcinoma. Cell Rep. 2020;33: 108276.

4. Ruiz-Andres O, Sanchez-Niño MD, Cannata-Ortiz P, Ruiz-Ortega M, Egido J, Ortiz A, et al. Histone lysine-crotonylation in acute kidney injury. Dis Models Mech. 2016. https://doi.org/10.1242/dmm.024455.

5. Minguez P, Parca L, Diella F, Mende DR, Kumar R, Helmer-Citterich M, et al. Deciphering a global network of functionally associated post-translational modifications. Mol Syst Biol. 2012;8:599.

6. Samanta L, Swain N, Ayaz A, Venugopal V, Agarwal A. Post-translational modifications in sperm proteome: the chemistry of proteome diversifications in the pathophysiology of male factor infertility. Biochim Biophys Acta Gen Sub. 2016;1860:1450–65.

7. Vu LD, Gevaert K, De Smet I. Protein language: post-translational modifications talking to each other. Trends Plant Sci. 2018;23:1068–80.

8. Bao X, Liu Z, Zhang W, Gladysz K, Fung YME, Tian G, et al. Glutarylation of histone H4 lysine 91 regulates chromatin dynamics. Mol Cell. 2019;76:660-675.e9.

9. Xie Z, Zhang D, Chung D, Tang Z, Huang H, Dai L, et al. Metabolic regulation of gene expression by histone lysine β-hydroxybutyrylation. Mol Cell. 2016;62:194–206.

10. Chen Y, Sprung R, Tang Y, Ball H, Sangras B, Kim SC, et al. Lysine propionylation and butyrylation are novel post-translational modifications in histones. Mol Cell Proteomics. 2007;6:812–9.

11. Zhang Z, Tan M, Xie Z, Dai L, Chen Y, Zhao Y. Identification of lysine succinylation as a new post-translational modification. Nat Chem Biol. 2011;7:58–63.

12. Xu W, Wan J, Zhan J, Li X, He H, Shi Z, et al. Global profiling of crotonylation on non-histone proteins. Cell Res. 2017;27:946–9.

13. Sun H, Liu X, Li F, Li W, Zhang J, Xiao Z, et al. First comprehensive proteome analysis of lysine crotonylation in seedling leaves of Nicotiana tabacum. Sci Rep. 2017;7:3013.

14. Yu AQ, Wang J, Jiang ST, Yuan LQ, Ma HY, Hu YM, et al. SIRT7-induced PHF5A decrotonylation regulates aging progress through alternative splicing-mediated downregulation of CDK2. Front Cell Dev Biol. 2021;9: 710479.

15. Sabari BR, Tang Z, Huang H, Yong-Gonzalez V, Molina H, Kong HE, et al. Intracellular crotonyl-CoA stimulates transcription through p300-catalyzed histone crotonylation. Mol Cell. 2015;58:203–15.

16. Sánchez-Tilló E, De Barrios O, Siles L, Cuatrecasas M, Castells A, Postigo A. β-catenin/TCF4 complex induces the epithelial-to-mesenchymal transition (EMT)-activator ZEB1 to regulate tumor invasiveness. Proc Natl Acad Sci USA. 2011;108:19204–9.

17. Zhong J, Liu C, Zhang QH, Chen L, Shen Y-Y, Chen Y-J, et al. TGF-β1 induces HMGA1 expression: the role of HMGA1 in thyroid cancer proliferation and invasion. Int J Oncol. 2017;50:1567–78.

18. Zhong J, Liu C, Chen Y, Zhang Q, Yang J, Kang X, et al. The association between S100A13 and HMGA1 in the modulation of thyroid cancer proliferation and invasion. J Transl Med. 2016;14:80.

19. Tan M, Luo H, Lee S, Jin F, Yang JS, Montellier E, et al. Identification of 67 histone marks and histone lysine crotonylation as a new type of histone modification. Cell. 2011;146:1016–28.

20. Martinez-Moreno JM, Fontecha-Barriuso M, Martín-Sánchez D, Sánchez-Niño MD, Ruiz-Ortega M, Sanz AB, et al. The contribution of histone crotonylation to tissue health and disease: focus on kidney health. Front Pharmacol. 2020;11:393.

21. Wu M-S, Li X-J, Liu C-Y, Xu Q, Huang J-Q, Gu S, et al. Effects of histone modification in major depressive disorder. CN. 2022;20:1261–77.

22. Fang Y, Xu X, Ding J, Yang L, Doan MT, Karmaus PWF, et al. Histone crotonylation promotes mesoendodermal commitment of human embryonic stem cells. Cell Stem Cell. 2021;28:748-763.e7.

23. Li D, Dewey MG, Wang L, Falcinelli SD, Wong LM, Tang Y, et al. Crotonylation sensitizes IAPi-induced disruption of latent HIV by enhancing p100 cleavage into p52. iScience. 2022;25:103649.

24. Liao W, Xu N, Zhang H, Liao W, Wang Y, Wang S, et al. Persistent high glucose induced EPB41L4A-AS1 inhibits glucose uptake via GCN5 mediating crotonylation and acetylation of histones and non-histones. Clin Transl Med. 2022;12: e699.

25. Xu X, Zhu X, Liu F, Lu W, Wang Y, Yu J. The effects of histone crotonylation and bromodomain protein 4 on prostate cancer cell lines. Transl Androl Urol. 2021;10:900–14.

26. Liao M, Chu W, Sun X, Zheng W, Gao S, Li D, et al. Reduction of H3K27cr modification during DNA damage in colon cancer. Front Oncol. 2022;12: 924061.

27. Zhang X, Chen J, Dong Q, Zhu J, Peng R, He C, et al. Lysine acylation modification landscape of Brucella abortus proteome and its virulent proteins. Front Cell Dev Biol. 2022;10: 839822.

28. Yu H, Bu C, Liu Y, Gong T, Liu X, Liu S, et al. Global crotonylome reveals CDYL-regulated RPA1 crotonylation in homologous recombination–mediated DNA repair. Sci Adv. 2020;6:eaay4697.

29. Zhang Y, Chen Y, Zhang Z, Tao X, Xu S, Zhang X, et al. Acox2 is a regulator of lysine crotonylation that mediates hepatic metabolic homeostasis in mice. Cell Death Dis. 2022;13:279.

30. Zhang D, Tang J, Xu Y, Huang X, Wang Y, Jin X, et al. Global crotonylome reveals hypoxia-mediated lamin A crotonylation regulated by HDAC6 in liver cancer. Cell Death Dis. 2022;13:717.

31. Qian Z, Ye J, Li J, Che Y, Yu W, Xu P, et al. Decrotonylation of AKT1 promotes AKT1 phosphorylation and activation during myogenic differentiation. J Adv Res. 2023;50:117–33.

32. Cai W, Xu D, Zeng C, Liao F, Li R, Lin Y, et al. Modulating lysine crotonylation in cardiomyocytes improves myocardial outcomes. Circ Res. 2022;131:456–72.

33. Huang J, Tang D, Zheng F, Xu H, Dai Y. Comprehensive analysis of lysine crotonylation modification in patients with chronic renal failure. BMC Nephrol. 2021;22:310.

34. Liu Y, Li Y, Liang J, Sun Z, Sun C. Non-histone lysine crotonylation is involved in the regulation of white fat browning. IJMS. 2022;23:12733.

35. Lao Y, Cui X, Xu Z, Yan H, Zhang Z, Zhang Z, et al. Glutaryl-CoA dehydrogenase suppresses tumor progression and shapes an anti-tumor microenvironment in hepatocellular carcinoma. J Hepatol. 2024;S0168827824003696.

36. Hou J-Y, Cao J, Gao L-J, Zhang F-P, Shen J, Zhou L, et al. Upregulation of α enolase (ENO1) crotonylation in colorectal cancer and its promoting effect on cancer cell metastasis. Biochem Biophys Res Commun. 2021;578:77–83.

37. Gao M, Wang J, Rousseaux S, Tan M, Pan L, Peng L, et al. Metabolically controlled histone H4K5 acylation/acetylation ratio drives BRD4 genomic distribution. Cell Rep. 2021;36: 109460.

38. Liang N, Mi L, Li J, Li T, Chen J, Dionigi G, et al. Pan-cancer analysis of the oncogenic and prognostic role of PKM2: a potential target for survival and immunotherapy. BioMed Res Int. 2023;2023:1–14.

39. Tian J, Luo B. Identification of three prognosis-related differentially expressed lncRNAs driven by copy number variation in thyroid cancer. J Immunol Res. 2022;2022:1–18.

40. Gil F, Miranda-Filho A, Uribe-Perez C, Arias-Ortiz NE, Yépez-Chamorro MC, Bravo LM, et al. Impact of the management and proportion of lost to follow-up cases on cancer survival estimates for small population-based cancer registries. J Cancer Epidemiol. 2022;2022:1–10.

41. Neto V, Esteves-Ferreira S, Inácio I, Alves M, Dantas R, Almeida I, et al. Metabolic profile characterization of different thyroid nodules using FTIR spectroscopy: a review. Metabolites. 2022;12:53.

42. Walenta JH, Didier AJ, Liu X, Krämer H. The golgi-associated Hook3 protein is a member of a novel family of microtubule-binding proteins. J Cell Biol. 2001;152:923–34.

43. Ciampi R, Giordano TJ, Wikenheiser-Brokamp K, Koenig RJ, Nikiforov YE. HOOK3-RET: a novel type of RET/PTC rearrangement in papillary thyroid carcinoma. Endocr Relat Cancer. 2007;14:445–52.

44. Melling N, Harutyunyan L, Hube-Magg C, Kluth M, Simon R, Lebok P, et al. High-level HOOK3 expression is an independent predictor of poor prognosis associated with genomic instability in prostate cancer. PLoS ONE. 2015;10:e0134614.

45. Gao S, Wang S, Zhao Z, Zhang C, Liu Z, Ye P, et al. TUBB4A interacts with MYH9 to protect the nucleus during cell migration and promotes prostate cancer via GSK3β/β-catenin signalling. Nat Commun. 2022;13:2792.

46. Liu L, Chen C, Liu P, Li J, Pang Z, Zhu J, et al. MYH10 combines with MYH9 to recruit USP45 by deubiquitinating snail and promotes serous ovarian cancer carcinogenesis, progression, and cisplatin resistance. Adv Sci. 2023;10:2203423.

Li *et al. Journal of Translational Medicine*   (2024) 22:874

Page 19 of 19

47. Li Q, Luo H, Dai F, Wang R, Fan X, Luo Y, et al. SAMD9 promotes postoperative recurrence of esophageal squamous cell carcinoma by stimulating MYH9-mediated GSK3 β / β -catenin signaling. Adv Sci. 2023;10:2203573.

48. Hu R, Cao Y, Wang Y, Zhao T, Yang K, Fan M, et al. TMEM120B strengthens breast cancer cell stemness and accelerates chemotherapy resistance via β1-integrin/FAK-TAZ-mTOR signaling axis by binding to MYH9. Breast Cancer Res. 2024;26:48.

49. Xu J, Wang J, He Z, Chen P, Jiang X, Chen Y, et al. LncRNA CERS6-AS1 promotes proliferation and metastasis through the upregulation of YWHAG and activation of ERK signaling in pancreatic cancer. Cell Death Dis. 2021;12:648.

50. Cao Z-Q, Wang Z, Leng P. Aberrant N-cadherin expression in cancer. Biomed Pharmacother. 2019;118: 109320.

Publisher's Note

Springer Nature remains neutral with regard to jurisdictional claims in published maps and institutional affiliations.